Fabrication of CdSnP$_2$ Thin Films by Phosphidation for Photovoltaic Application

Shigeru Nakatsuka*, Ryosuke Inoue and Yoshitaro Nose

Department of Materials Science and Engineering, Kyoto University, Kyoto 606-8501, Japan

Keywords: II-IV-V$_2$, chalcopyrite, CdSnP$_2$, ZnSnP$_2$, phosphidation

* To whom all correspondence should be addressed. Tel.: +81-75-753-5472; Fax: +81-75-753-3579; E-mail: nakatsuka.shigeru.25c@kyoto-u.jp

Abstract

We report on the fabrication of $CdSnP_2$ thin films for photovoltaic application. The phosphidation method, where co-sputtered Cd-Sn precursor thin film reacts with phosphorus gas, was utilized for the preparation of $CdSnP_2$ thin films. In order to establish the fabrication process, the temperature dependence on product phases was investigated and $CdSnP_2$ thin films were obtained by the phosphidation at 350 °C for 30 min under the phosphorus vapor pressure of 10^{-2} atm. $CdSnP_2$ thin films showed a n-type conduction. The resistivity, the carrier concentration and the mobility were evaluated to be $3.5-3.7 \times 10^2$ Ω cm, $1-3 \times 10^{15}$ cm^{-3} and $4.7-17$ cm^2 V^{-1} s^{-1}, respectively. $CdSnP_2$ thin films with relatively flat and smooth surface were obtained, although it was reported that $ZnSnP_2$ with the same crystal structure grew as the protrusion shape by the VLS growth mode. In order to investigate these difference in growth mechanism between $CdSnP_2$ and $ZnSnP_2$, the reaction process in Cd-Sn-P system was investigated and discussed based on the chemical potential diagrams. As the result, it was understood that Cd, Sn and P_4 directly reacted to form $CdSnP_2$, while $ZnSnP_2$ was formed via the reaction among Zn_3P_2, Sn and P_4 after Zn reacts with P_4 to produce Zn_3P_2. Therefore, it is speculated that simple reaction route results in the high growth speed and smooth flat morphology was obtained in the fabrication of $CdSnP_2$ thin films.

.

1. Introduction

CuIn$_{1-x}$Ga$_x$Se$_2$ (CIGS) and CdTe are promising materials for thin film photovoltaic devices. The solar cells based on these chalcogenide compounds recorded the high conversion efficiencies of 22.6 %[1] for CIGS and 22.1 %[2] for CdTe, respectively. However, the usage of rare or toxic elements prevents the widespread use of these compound semiconductors. From these backgrounds, materials composed of non-toxic and earth-abundant elements have been researched and Cu$_2$ZnSnS$_{4-x}$Se$_x$ achieved the high conversion efficiency of 12.6 %.[3] In addition, Cu$_2$SnS$_3$,[4] Cu$_2$O,[5] SnS,[6] FeS$_2$,[7] and Zn$_3$P$_2$[8] have been also investigated for the same concept.

ZnSnP$_2$ is also a promising material for solar absorber consisting of safe and earth-abundant elements. In the previous works, it was reported that ZnSnP$_2$ showed a p-type conduction with the carrier concentration of 10^{16}–10^{18} cm^{-3} and a direct bandgap of ~ 1.6 eV.[9–16] Based on Shockley-Queisser limit,[17] the theoretical conversion efficiency of about 30% is calculated in the single-junction solar cell using ZnSnP$_2$ under the condition of AM 1.5 G solar spectrum.[18] The absorption coefficient of ZnSnP$_2$ was reported to be approximately 10^5 cm^{-1} in visible light range,[18,19] which is comparable to that of CIGS.[18,20] Our research group reported that solar cells using ZnSnP$_2$ thin films[21] and bulk crystals [15,22,23]. The solar cells using ZnSnP$_2$ bulk crystals recorded the best conversion

1   efficiency of 3.44 % (J_{SC} = 12.3 mA/cm^2, V_{OC} = 0.472 V, FF = 0.594).[23] The solar cell

2   structure was Al/ZnO;Al/ZnO/(Cd,Zn)S/ZnSnP$_2$/Cu. In this device, the value of V_{OC} was

3   largely low considering the bandgap of ZnSnP$_2$. XPS measurements revealed that

4   CdS/ZnSnP$_2$ showed a large conduction band offset, ΔE_C = −1.2 eV,[24] which suggested

5   that band alignment was− necessary to achieve a high conversion efficiency.

6   In this study, we focused on CdSnP$_2$ as a n-type material in the ZnSnP$_2$ solar cells.

7   CdSnP$_2$ has a chalcopyrite structure as well as ZnSnP$_2$ and its bandgap is 1.17 eV.[25]

8   Kumagai $et\ al.$ carried out the first-principles calculation in ZnSnP$_2$ with chalcopyrite

9   structure to obtain its band structure.[26] They reported that the valence band maximum

10   (VBM) at the Γ point is mainly composed of P orbitals with slight hybridization with Zn

11   and Sn orbitals and the conduction band minimum (CBM) is primarily composed of Zn

12   and Sn cations orbitals. Consequently, the level of VBM in CdSnP$_2$ might be similar to

13   that in ZnSnP$_2$ because of the same crystal structure and anions. This results in the ΔE_C

14   value of − 0.5 eV between ZnSnP$_2$ and CdSnP$_2$ considering the difference of bandgap in

15   both compounds and the improvement of band alignment is expected compared to CdS.

16   In addition, it was reported that ZnSnP$_2$ and CdSnP$_2$ form a solid solution in all

17   composition range,[27] which suggests the intermixing of Zn and Cd atoms at

18   CdSnP$_2$/ZnSnP$_2$ interface and pn-junction with few band offset and interfacial defect can

1   be formed. However, few reports on the formation of $CdSnP_2$ thin films are available.

2   In this report, we thus tried to establish the fabrication process to obtain $CdSnP_2$ thin

3   films, where Cd-Sn precursor thin films react with phosphorus gas, so-called

4   phosphidation. Particularly, the impact of reaction temperature on product phases was

5   investigated and morphology change was discussed based on the chemical potential

6   diagrams.

7   **2. Experimental method**

8   Cd-Sn thin films with the thickness of 0.5 μm were fabricated as a precursor on soda

9   lime glass substrates by magnetron direct current sputtering with a base pressure of

10   5×10^{-4}Pa. The 1 inch target materials of Cd (99.9 %, Kojundo Chemical Laboratory) and

11   Sn (99.99%, Furuuchi Chemical) were co-sputtered for 45 min under an Ar atmosphere

12   with the pressure of 0.8 Pa and the gas flow rate of 20 sccm. The power densities for Cd

13   and Sn targets were set at 0.6 and 3.2 W/cm^2, respectively. During the sputtering, the

14   substrates were rotated at 12 rpm without heating. For the safety sputtering of Cd, the

15   target materials were sufficiently cooled down for more than 30 min. Dust collecting

16   should be utilized when sample are extracted from a sputtering chamber. The thickness

17   and composition were measured by inductively coupled plasma-atomic emission

18   spectroscopy (ICP-AES, SII Nano Technology SPS3520UV). The samples were

1 dissolved in inverse aqua regia (HNO_3:HCl = 3:1) and the solution 1/10 diluted with

2 deionized water was used for the ICP-AES measurements. Considering the higher vapor

3 pressure of Cd, the molar ratio [Cd]/[Sn] was controlled to be about 1.2 in the precursor

4 thin films.

5 Then, Cd-Sn thin films reacted with phosphorus gas to obtain $CdSnP_2$ thin films by

6 phosphidation. The details of the experimental conditions were described in our previous

7 work.[28] We used two phase sample with Sn and Sn_4P_3 as a phosphorus source and

8 phosphorus gas was transported to the precursor thin films using Ar carrier gas, which

9 was deoxidized by passing through a Ti sponge heated at 900 °C. The partial pressure of

10 phosphorus was set at approximately 10^{-2} atm by controlling the temperature of two phase

11 sample. In this study, the phosphidation temperatures were 300, 350 and 400 °C. After

12 the phosphidation, the thin films were cooled down in the furnace by turning off the heater,

13 or quenched outside the furnace. The surficial and cross-sectional morphology of thin

14 films before and after phosphidation were analysed by scanning electron microscopy

15 (SEM, HITACHI S-3500H and HITACHI SU-1500) The product phases were identified

16 by X-ray diffraction (XRD, Panalytical X'Pert Pro Alpha-1), where $CuK\alpha1$ (λ=1.5406

17 Å) was used as an incident X-ray (45 kV,40 mA) in Bragg–Brentano (θ–2θ) configuration.

18 In order to evaluate the electrical properties, Hall effect and resistivity measurements

1   were carried out at room temperature based on van der Pauw method using Hall-resistivity

2   measurement system (Toyo Technica, ResiTest8300).

3   For the consideration of growth mechanism in the phosphidation method, we used the

4   chemical potential diagrams. The review on the chemical potential diagrams is well

5   summarized by Yokokawa.[29] A chemical potential diagram shows a stable potential

6   region in various substances and each axis represents a chemical potentials of constituent

7   elements. The chemical potential diagram of the Cd-Sn-P system was drawn using the

8   software, Chesta 3.2.6.9, developed by Hatada. In order to obtain the potential diagrams,

9   the thermodynamic data for Cd (g) and Sn (g) were derived from the database edited by

10   Barin[30]. The Gibbs energies of formation for CdP_2 (s), Cd_3P_2 (s) and $CdSnP_2$ (s) reported

11   by Sirota *et al.*[31] and Smolyarenko *et al.*[32] were also utilized.

12   **3. Results and discussion**

13   **3.1. Effect of phosphidation temperature**

14   In order to obtain $CdSnP_2$ thin films with the single-phase, the phosphidation of Cd-Sn

15   precursor thin films was carried out at various reaction temperatures such as 300, 350 and

16   400 °C. In each experiment, Cd-Sn precursor thin films reacted with phosphorus gas for

17   30 min and then was cooled down in the furnace. Figure 1 shows the XRD profiles of Cd-

18   Sn precursor thin films before and after phosphidation. In the precursor thin film, Cd and

1 Sn were identified and alloy was not observed, because Cd-Sn system is a typical eutectic

2 system. The formation of $CdSnP_2$ as a main phase was observed in the phosphidation at

3 300 and 350 °C. In particular, all reflections observed in the sample prepared at 350 °C

4 were corresponded to the reflections of $CdSnP_2$. In addition, those samples show (112)

5 plane orientation of $CdSnP_2$, which is a close-packed plane in chalcopyrite structure. ICP-

6 AES analysis showed that the composition of the thin film fabricated at 350 °C was 27.2

7 at. % Cd, 23.6 at. % Sn and 53.2 at.% P, which is Cd-rich composition compared with the

8 stoichiometric ratio of $CdSnP_2$. In some samples prepared by the same condition, Cd_3P_2

9 was identified from XRD profiles. Therefore, the existence of Cd_3P_2 as a secondary phase

10 is considered even in the case that Cd_3P_2 is not identified in XRD profiles as shown in

11 Fig. 1. While, Cd_6P_7 and Sn were identified in addition to $CdSnP_2$ in the sample for 400

12 °C.

13 Figure 2 shows SEM images of Cd-Sn precursor thin films before and after

14 phosphidation. The Cd-Sn precursor thin film was composed of sub-micron particles. On

15 the other hand, the sub-micron particles were not observed in the thin film after

16 phosphidation at 300 °C, which was the morphology indicating that metal precursor

17 melted. The phosphidation at 350 °C resulted in the $CdSnP_2$ thin film consisting of

18 particles with the diameter of about 1 μm. The particles with the diameter of a few μm

1   were formed on the surface of the thin film in the sample after phosphidation at 400 °C.

2   Such particles might be secondary phases containing Sn. The cross-sectional SEM

3   observation was carried out in Cd-Sn precursor thin film and $CdSnP_2$ thin film fabricated

4   by the phosphidation at 350 °C as shown in Fig. 3. In the Cd-Sn precursor thin film, it is

5   observed that sub-micron particles were deposited on the glass substrate, while $CdSnP_2$

6   film shows the dense microstructure consisting of granular particles compared with the

7   Cd-Sn precursor thin film. This implies that phosphidation reaction proceeded as metal

8   precursor partly-melted. In addition, it is confirmed that the thickness of the film was

9   reduced, which might be attributed to the evaporation of precursor metal. ICP-AES

10   analysis also clarified that a half amount of precursor metal, Cd and Sn, evaporated during

11   the phosphidation experiments at 350 °C, which has to be improved in future work. The

12   Hall measurement indicates that $CdSnP_2$ thin films prepared by the phosphidation has the

13   *n*-type conduction as well as the $CdSnP_2$ bulk crystals grown by the solution method.[25]

14    $CdSnP_2$ thin films showed a *n*-type conduction. The resistivity, the carrier concentration

15   and the mobility were evaluated to be $3.5-3.7\times10^2$ Ω cm, $1-3\times10^{15}$ cm^{-3} and $4.7-17$ cm^2

16   V^{-1} s^{-1}, respectively.

17   As mentioned above, $CdSnP_2$ thin films were obtained by the phosphidation of Cd-Sn

18   precursor thin films at 350 °C for 30 min. In addition, $CdSnP_2$ thin films has relatively

1   smooth morphology compared with $ZnSnP_2$ thin films. In our previous work, a different

2   surface morphology was observed in $ZnSnP_2$ thin films fabricated even by a similar

3   phosphidation process.[28] Some $ZnSnP_2$ protrusions with the length of a few μm were

4   formed on the $ZnSnP_2$ thin film by so-called VLS (Vapor-Liquid-Solid) growth mode.[28,33]

5   It is interesting that $CdSnP_2$ and $ZnSnP_2$ showed different morphologies in spite of the

6   similarity in constituent elements and crystal structures.

7   **3.2. Growth mechanism of $CdSnP_2$ thin film**

8   The time dependence of phosphidation in $CdSnP_2$ was investigated in order to clarify

9   the growth mechanism. Here, we prepared a sample discontinued at 250 °C on the way

10   heating up to 300 °C and another one after the phosphidation of Cd-Sn thin film at 300

11   °C for 2 min. Each sample was quenched outside the furnace in order to freeze the state

12   during the phosphidation, while samples as shown in the previous section were

13   conventionally cooled in the furnace after phosphidation. Figure 4 shows the XRD profile

14   for each sample. The discontinued sample indicates that phosphidation reaction had not

15   started at the heating stage because precursor metals such as Cd and Sn were identified.

16   On the other hand, $CdSnP_2$ is observed as a main phase even in the phosphidation for 2

17   min, which suggests that the reaction rate to form $CdSnP_2$ is higher compared with

18    $ZnSnP_2$ fabricated by the same phosphidation method. In the case of $ZnSnP_2$, 5 min

1   phosphidation did not finish the formation of $ZnSnP_2$ even in the higher reaction

2   temperature of 450 °C. It is also understood that partly-melted precursor metal is an

3   important factor for fast phosphidation reaction from the SEM images of the film surface

4   shown in Figure 5, as previously predicted.

5   Here, the difference of the surface morphologies between $CdSnP_2$ and $ZnSnP_2$ films is

6   discussed. In this study, we consider the difference in growth mechanism between both

7   based on the chemical potential diagrams, because the morphology might depend on the

8   growth mechanism of each thin film. Figure 6 shows the chemical potential diagrams of

9   the Cd-Sn-P system at 300 °C together with the diagram of the Zn-Sn-P system at 450 °C,

10   which was previously reported by our group. [28] The logarithms of the partial pressures of

11   Cd (g), Zn (g), Sn (g) and P_4 (g) were used as the axes, which represent their chemical

12   potentials. The dotted line indicates the partial pressure of P_4 (g) controlled in the

13   experiments: 10^{-2} atm.

14   We discuss the phosphidation process of Cd-Sn precursor thin films as well as the case

15   of Zn-Sn films. The point A in Figure 6a represents the state for Cd-Sn precursor thin

16   films before phosphidation. Then, the chemical potential of phosphorus in the film

17   increases with keeping the equilibrium of Cd (l) and Sn (l) as the phosphidation reaction

18   proceeds, and at the point B, $CdSnP_2$ (s) forms. On the other hand, in the Zn-Sn-P system

1 shown in Figure 6b, the phosphorus potential for the formation of $ZnSnP_2$ (s) shown by

2 point D is much higher than that for Zn_3P_2 (s) shown by point C. It is thus understood that

3 the formation of Zn_3P_2 (s) preferentially occurs before $ZnSnP_2$ (s) in the Zn-Sn-P system.

4 Such a behaviour was experimentally observed in our previous work.[28] The previous

5 work also showed that the surface morphology of $ZnSnP_2$ thin films was rough and some

6 protrusions were grown. To discuss the roughness of $ZnSnP_2$ thin films, two issues during

7 phosphidation should be considered. One is the microstructure of the Zn-Sn precursor

8 thin films before phosphidation, where it was observed that the separation of Zn and Sn

9 grains and the cohesion of Sn with the grain size of a few micron. The separation is

10 expected from the phase diagram of the Zn-Sn system. The other one is a phosphidation

11 process, which was investigated experimentally and thermodynamically. The formation

12 of $ZnSnP_2$ protrusions by VLS growth mode is due to the above two issues. On the other

13 hand, the grain size in Cd-Sn precursor thin films is sub-micron as shown in Figure 2a

14 although the separation of Cd and Sn is observed. In addition, the equilibrium chemical

15 potential of phosphorus with $CdSnP_2$ is lower than that with Cd_3P_2 as shown in Figure 6a,

16 which suggests that $CdSnP_2$ forms without the formation of other phases as described

17 above. These are different with the case of $ZnSnP_2$, and key conditions to obtain a smooth

18 surface of $CdSnP_2$ films.

4. Conclusions

In this study, we investigated the temperature dependence in phosphidation of Cd-Sn thin films on product phases and $CdSnP_2$ thin films were prepared at 350 °C for 30 min under the phosphorus vapor pressure of 10^{-2} atm. $CdSnP_2$ thin films showed a n-type conduction. $CdSnP_2$ thin films showed a n-type conduction. The resistivity, the carrier concentration and the mobility were evaluated to be $3.5-3.7 \times 10^2$ Ω cm, $1-3 \times 10^{15}$ cm^{-3} and $4.7-17$ cm^2 V^{-1} s^{-1}, respectively. The SEM observation suggested that $CdSnP_2$ thin films with relatively flat and smooth surface were obtained, although the formation of $ZnSnP_2$ protrusions by the VLS growth mode was reported in the case of the Zn-Sn-P system. In order to investigate the difference in both systems, the reaction process in the Cd-Sn-P system was investigated and discussed based on the chemical potential diagrams. The experimental results and the chemical potential diagram suggested that Cd, Sn and P_4 directly reacted to form $CdSnP_2$, while $ZnSnP_2$ was formed via the reaction among Zn_3P_2, Sn and P_4 after Zn reacts with P_4 to produce Zn_3P_2. Therefore, it is concluded that direct reaction route to form $CdSnP_2$ results in the high growth rate and flat morphology in the fabrication of $CdSnP_2$ thin films.

1 **Acknowledgements**

References

(1)   Jackson, P.; Wuerz, R.; Hariskos, D.; Lotter, E.; Witte, W.; Powalla, M. Effects of

        Heavy Alkali Elements in Cu(In,Ga)Se$_2$ Solar Cells with Efficiencies up to 22.6%.

        Phys. Status Solidi RRL **2016**, *10*, 583‑586.

(2)   First Solar. Fist Solar Hits Record 22.1% Conversion Efficiency for CdTe Solar

        Cell.   https://www.greentechmedia.com/articles/read/First-Solar-Hits-Record-

        22.1-Conversion-Efficiency-For-CdTe-Solar-Cell (last accessed January 2018).

(3)   Wang, W.; Winkler, M. T.; Gunawan, O.; Gokmen, T.; Todorov, T. K.; Zhu, Y.;

        Mitzi, D. B. Device Characteristics of CZTSSe Thin-Film Solar Cells with 12.6%

        Efficiency. *Adv. Energy Mater.* **2014**, *4*, 1301465.

(4)   Nakashima, M.; Fujimoto, J.; Yamaguchi, T.; Izaki, M. Cu$_2$SnS$_3$ Thin-Film Solar

        Cells Fabricated by Sulfurization from NaF/Cu/Sn Stacked Precursor. *Appl. Phys.*

        Express **2015**, *8*, 42303.

(5)   Minami, T.; Nishi, Y.; Miyata, T. Heterojunction Solar Cell with 6% Efficiency

        Based on an N-Type Aluminum-Galium-Oxide Thin Film and P-Type Sodium-

        Doped Cu$_2$O Sheet. *Appl. Phys. Express* **2015**, *8*, 22301.

(6)   Sinsermsuksakul, P.; Sun, L.; Lee, S. W.; Park, H. H.; Kim, S. B.; Yang, C.;

        Gordon, R. G. Overcoming Efficiency Limitations of Sn-S-Based Solar Cells. *Adv.*

Energy Mater. **2014**, *4 , 1400496.*

(7)   Ennaoui, A.; Tributsch, H. Iron Sulphide Solar Cell. *Sol. Cells* **1984**, *13*, 197‑200.

(8)   Bhushan, M.; Catalano, A. Polycrystalline Zn3P2 Schottky Barrier Solar Cells. *ppl. Phys. Lett.* **1981**, *38*, 39‑41.

(9)   Abdurakhimov, A. A.; Kradinova, L. V.; Parimbekov, Z. A.; Rud', Y. V. chottky Diodes Made of P-Type ZnSnP2. *Sov. Phys. Semicond.* **1982**, *16*, 156‑59.

(10)   Ryan, M. A.; Peterson, M. W.; Williamson, D. L.; Frey, J. S.; Maciel, G. E.; arkinson, B. A. Metal Site Disorder in Zinc Tin Phosphide. *J. Mater. Res.* **1987**, , 528‑537.

(11)   Nakatsuka, S.; Nakamoto, H.; Nose, Y.; Uda, T.; Shirai, Y. Bulk Crystal Growth nd Characterization of $ZnSnP_2$ Compound Semiconductor by Flux Method. *Phys. Status Solidi C* **2015**, *12*, 520‑523.

(12)   Scanlon, D. O.; Walsh, A. Bandgap Engineering of $ZnSnP_2$ for High-Efficiency Solar Cells. *Appl. Phys. Lett.* **2012**, *100*, 251911.

(13)   Hinuma, Y.; Oba, F.; Nose, Y.; Tanaka, I. First-Principles Study of Valence Band Offset at $ZnSnP_2$/CdS, $ZnSnP_2$/ZnS, and Related Chalcopyrite/Zincblende Heterointerfaces. *J. Appl. Phys.* **2013**, *114*, 043718.

(14)   Ajmera, P. K.; Shin, H. Y.; Zamanian, B. Vacuum Growth of Thin Films of $ZnSnP_2$.

Sol. Cells **1987**, *21*, 291‑299.

(15) Nakatsuka, S.; Yuzawa, N.; Chantana, J.; Minemoto, T.; Nose, Y. Solar Cells

Using Bulk Crystals of Rare Metal-Free Compound Semiconductor $ZnSnP_2$. *Phys.*

Status Solidi A **2017**, *214*, 1600650.

(16) Nakatani, K.; Minemura, T.; Miyauchi, K.; Fukabori, K.; Nakanishi, H.; Sugiyama,

M.; Shirakata, S. Photoluminescence Property of $ZnSnP_2$ by Solution Growth and

Normal Freezing Methods. *Jpn. J. Appl. Phys.* **2008**, *47*, 5342–5344.

(17) Shockley, W.; Queisser, H. J. Detailed Balance Limit of Efficiency of PN Junction

Solar Cells. *J. Appl. Phys.* **1961**, *32*, 510‑519.

(18) Yokoyama, T.; Oba, F.; Seko, A.; Hayashi, H.; Nose, Y.; Tanaka, I. Theoretical

Photovoltaic Conversion Efficiencies of $ZnSnP_2$, $CdSnP_2$, and $Zn_{1-x}Cd_xSnP_2$

Alloys. *Appl. Phys. Express* **2013**, *6*, 61201.

(19) Shin, H. Y.; Ajmera, P. K. Characterization of Vacuum Grown Thin Films of

$ZnSnP_2$. *Mater. Lett.* **1987**, *5*, 211‑214.

(20) Minoura, S.; Kodera, K.; Maekawa, T.; Miyazaki, K.; Niki, S.; Fujiwara, H.

Dielectric function of $Cu(In,Ga)Se_2$-Based Polycrystalline Materials. *J. Appl. Phys.*

2013, *113*, 63505.

(21) Yuzawa, N.; Chantana, J.; Nakatsuka, S.; Nose, Y.; Minemoto, T. $ZnSnP_2$ thin-

film solar cell prepared by phosphidation method under optimized Zn/Sn atomic ratio of its absorbing layer. *Curr. Appl. Phys.* **2017**, *17* , 557–564.

(22)   Nakatsuka, S.; Akari, S.; Chantana, J.; Minemoto, T.; Nose, Y. Impact of Heterointerfaces in Solar Cells Using ZnSnP$_2$ Bulk Crystals. *ACS Appl. Mater. Interfaces* **2017**, *9*, 33827–33832.

(23)   Akari, S.; Chantana, J.; Nakatsuka, S.; Nose, Y.; Minemoto, T. ZnSnP$_2$ Solar Cell with (Cd,Zn)S Buffer Layer: Analysis of Recombination Rates. *Sol. Energy Mater. Sol. Cells* **2018**, *174,* 412–417.

(24)   Nakatsuka, S.; Nose, Y.; Shirai, Y. Band Offset at the Heterojunction Interfaces of CdS/ZnSnP$_2$, ZnS/ZnSnP$_2$, and In$_2$S$_3$/ZnSnP$_2$. *J. Appl. Phys.* **2016**, *119*, 193107.

(25)   Shay, J. L.; Wernick, J. H. *Chalcopyrite Semiconductors: Growth, Electronic Properties, and Applications*; Pergamon Press: Oxford, 1975.

(26)   Kumagai, Y.; Choi, M.; Nose, Y.; Oba, F. *Phys. Rev. B* First-principles study of point defects in chalcopyrite ZnSnP2. *Condens. Matter Mater. Phys.* **2014**, *90*, 1‑12.

(27)   Higashino, T.; Nose, Y.; Toyoura, K.; Uda, T. *Bulk Crystal Growth of Chalcopyrite Semiconductors of the Zn-Cd-Sn-P System Based on the Phase Diagram*. MRS Fall Meeting, Boston, USA, Nov 28−Dec 2, 2011.

(28)   Nakatsuka, S.; Nose, Y.; Uda, T. Fabrication of ZnSnP2 thin films by

phosphidation. *Thin Solid Films* **2015**, *589*, 66‑71.

(29)   Yokokawa, H. Generalized Chemical Potential Diagram and Its Applications to

Chemical Reactions at Interfaces Between Dissimilar Materials. *J. Phase*

Equilibria **1999**, *20*, 258‑287.

(30)   Barin, I. *Thermochemical Data of Pure Substances, third ed.*; VCH

Verlagsgesellschaft GmbH: Weinheim, 1995.

(31)   Sirota, N. N., Antyukhov, A. M., Smolyarenko, E. M. Investigation into

Thermodynamic Properties of Cd-P System Compound by Electromotive Forces

Method. *Dokl. Akad. Nauk SSSR* **1974**, *219*, 397.

(32)   Smolyarenko, E. M. Yakimovich, V. N. Thermodyanamics of Formation of

ZnSnP$_2$ and CdSnP$_2$. *Izv. Akad. Nauk SSSR, Neorg. Mater* **1981**, *17*, 132‑134.

(33)   Wagner, R. S.; Ellis, W. C. Vapor-Liquid-Solid Mechanism of Single Crystal

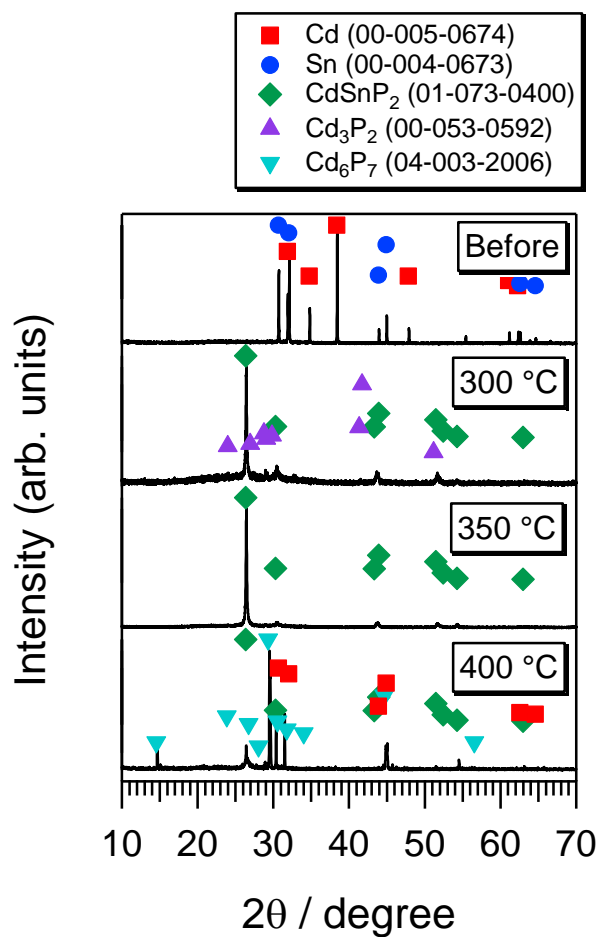Growth. *Appl. Phys. Lett.* **1964**, *4*, 89–90.

■ Figure captions

Figure 1. XRD profiles of Cd-Sn thin films before and after phosphidation for 30 min at various temperaturese.

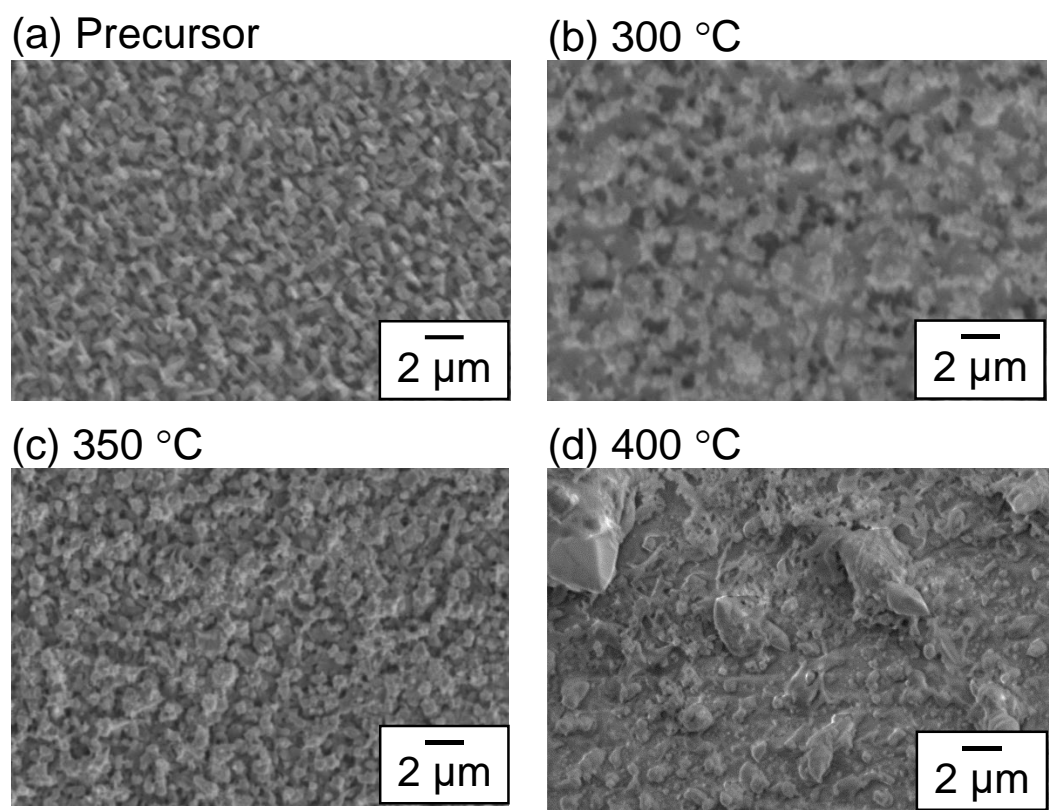Figure 2. SEM images of Cd-Sn thin films before and after phosphidation for 30 min at various temperatures.
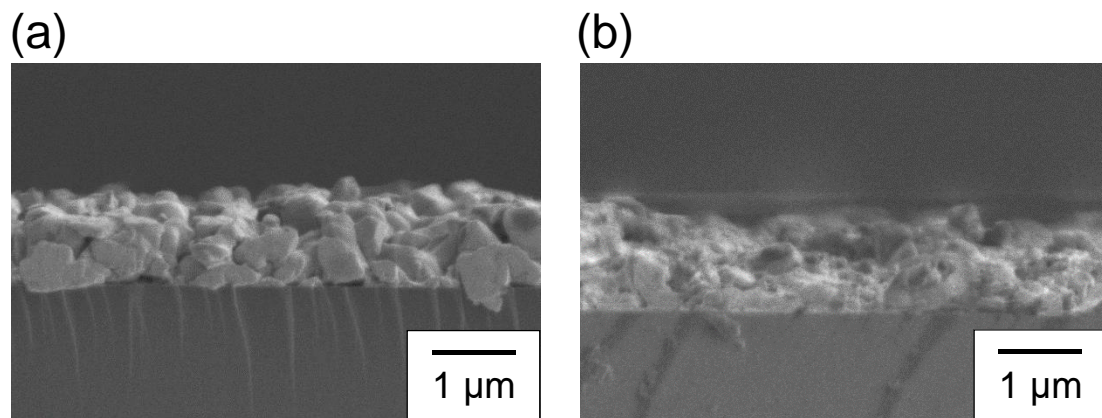
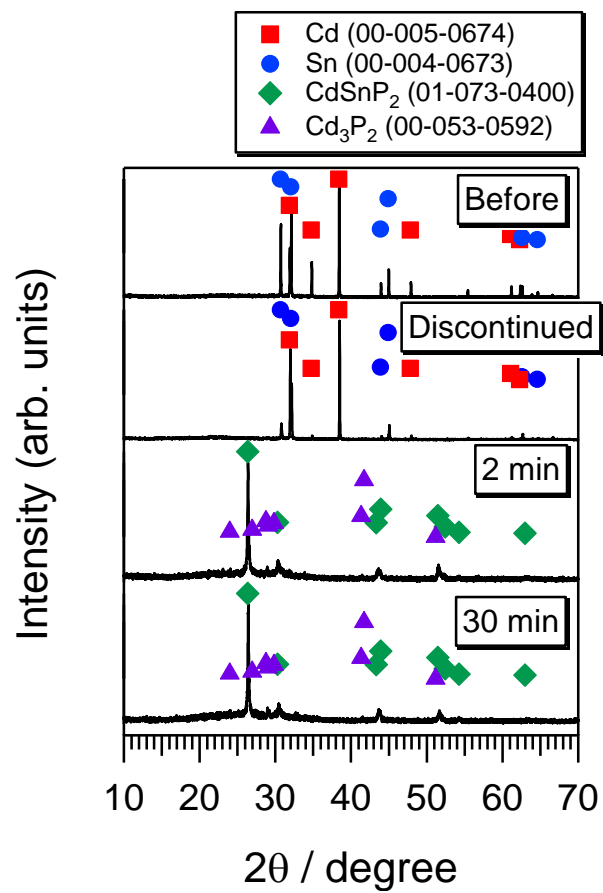Figure 3. Cross-sectional SEM images of Cd-Sn thin films (a) before and (b) after phosphidation at 350 °C.

Figure 4. XRD profiles of Cd-Sn thin films before and after phosphidation at 300 °C. "Discontinued" indicates the sample discontinued on the way heating up to 300 °C.
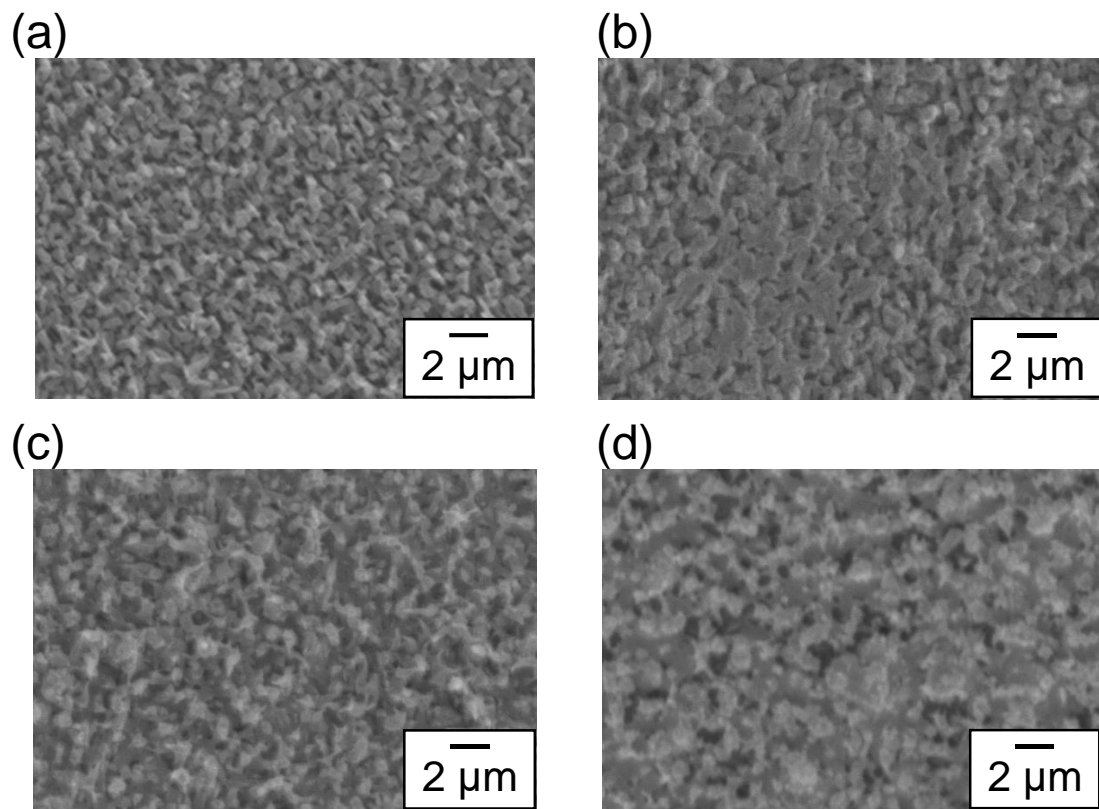
Figure 5. SEM images of thin films (a) before phosphidation, (b) discontinued during heating up, and after phosphidation at 300 °C (c) 5 min and (d) 30 min.

Figure 6. Chemical potential diagrams of (a) Cd-Sn-P system at 300 °C and (b) Zn-Sn-P system at 450 °C.

■ Figures

Fig. 1. XRD profiles of Cd-Sn thin films before and after phosphidation for 30 min at various temperaturese.

(a) Precursor

(b) 300 °C

2 µm

2 µm

(c) 350 °C

(d) 400 °C

2 µm

2 µm

Fig. 2. SEM images of Cd-Sn thin films before and after phosphidation for 30 min at various temperatures.

(a)

(b)

Fig. 3. Cross-sectional SEM images of Cd-Sn thin films (a) before and (b) after phosphidation at 350 °C.

Fig. 4. XRD profiles of Cd-Sn thin films before and after phosphidation at 300 °C.

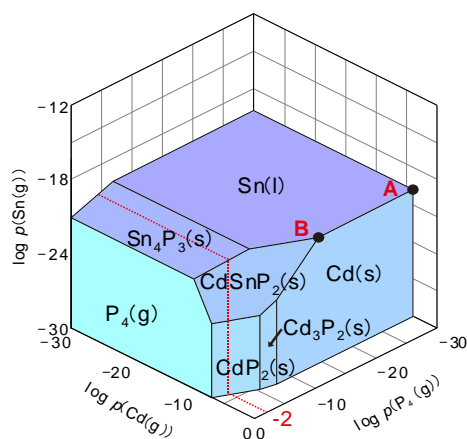"Discontinued" indicates the sample discontinued on the way heating up to 300 °C.

Fig. 5. SEM images of thin films (a) before phosphidation, (b) discontinued during heating up, and after phosphidation at 300 °C (c) 5 min and (d) 30 min.
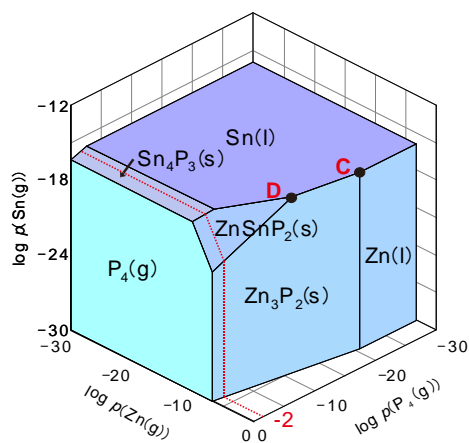
Fig. 6. Chemical potential diagrams of (a) Cd-Sn-P system at 300 °C and (b) Zn-Sn-P system at 450 °C.

■ Table of Contents (TOC) Image